Solar Energy 177 (2019) 229–240

Contents lists available at ScienceDirect

Solar Energy

journal homepage: www.elsevier.com/locate/solener

An analysis for S-shaped *I-V* characteristics of organic solar cells using lumped-parameter equivalent circuit model

Fei Yu*, Gongyi Huang, Wei Lin, Chuanzhong Xu

College of Information Science and Engineering, Huaqiao University, Xiamen 361021, China

ARTICLE INFO

Keywords:
Organic solar cells (OSCs)
Lumped-parameter model
OSC simulations
S-shaped current-voltage (*I-V*) characteristics
S-shaped kink

ABSTRACT

A lumped-parameter equivalent circuit model of organic solar cells (OSCs) is proposed to analyze the S-shaped current-voltage (*I-V*) characteristics and the explicit solution to *I-V* equation is derived so that this model is suitable to be compactly implemented for the simulations of photovoltaic applications. Comparing our explicit solutions with the method of least squares and the Newton-Raphson root-finding scheme, the simulations quantificationally reproduce the S-shaped *I-V* characteristics of OSCs especially for both linear- and exponential-like S-shaped kink in the third and first quadrants, respectively. Simultaneously, the simulations facilitate us to qualitatively analyze the S-shaped *I-V* characteristics of OSCs influenced by the different model parameters. Furthermore, we verify the simulation results of our proposed model by using the reconstructed experimental data. Good agreements indicate that such a model can be used to accurately predict the S-shaped *I-V* characteristics of OSCs and regarded as a serviceable tool implemented compactly into simulations of the wide photovoltaic applications.

1. Introduction

Today, electronic devices are facing a disruptive evolution, developing from heavy and rigid appliances to light and flexible devices. As the most promising next generation electronic devices, organic devices, such as organic thin-film transistors (OTFTs) and organic solar cells (OSCs), are mainly intended for low-cost, large-area, and flexible applications. Up to date, OSCs are still in the intensive researches (Tran et al., 2017; Sanchez et al., 2017; Dominguez et al., 2017) for suppressing S-shaped *I-V* characteristics (Wagenpfahl et al., 2010) to achieve high power-conversion efficiency (PCE) comparable to the conventional silicon-based solar cells (Chavali et al., 2017; Kale and Solanki, 2015; Yoshikawa et al., 2017). Therefore, an important requirement for the OSC applications in the engineering field is to have lumped-parameter equivalent circuit models that can be compactly implemented into simulators to predict and optimize the performances of OSCs.

The operating principle of OSCs is qualitatively similar as that of silicon-based solar cells, but the anomalous S-shaped kink observed in OSCs' *I-V* characteristics impairs the J-shaped *I-V* curve and PCE. Because the earlier conventional lumped-parameter models (Ortiz-Conde et al., 2014) including single diode failed in describing the S-shaped kink, multiple-diode lumped-parameter models (Mazhari, 2006; De Castro et al., 2010; Zuo et al., 2014; Kumar and Gaur, 2013; Gaur and Kumar, 2014; García-Sánchez et al., 2013; De Castro et al., 2016; Roland et al., 2016; Xu et al., 2018; Huang et al., 2018) are proposed to give some reasonable explanations on it from the view of electricity. Mazhari (2006) understood the incapacity of single-diode models in describing the S-shaped kink and suggested that two more diodes are used to produce the non-constant photo-current and concave S-shaped behavior, respectively. Up to now, Mazhari's model (Mazhari, 2006) is the simplest circuit in all of the above three-diode models because the least fitting parameters are required for simulations. Of course, the improvement rooms on efficiency and accuracy of computing Mazhari's model are still left for us. B. Mazhari's model (Mazhari, 2006) is unable to model the linear-like rise S-shaped kink in the third quadrant due to the absence of resistance Xu et al. (2018) and Huang et al. (2018). De Castro et al. (2010) and Zuo et al. (2014) proposed two-diode lumped-parameter models, which cannot demonstrate Heterojunction OSCs' S-shaped kink with the exponential-like rise in the first quadrant. Kumar and Gaur (2013) and Gaur and Kumar (2014) proposed two improved equivalent circuit models to represent the behavior of polymer solar cells under different environmental conditions, but these two models do not result in a compact formulation. García-Sánchez et al. (2013) dealed with the inability of F. Araujo de Castro's model by adding another diode, which allows the experimentally observed exponential-like

* Corresponding author.
E-mail address: yufei_jnu@126.com (F. Yu).

https://doi.org/10.1016/j.solener.2018.11.011
Received 6 September 2018; Received in revised form 23 October 2018; Accepted 3 November 2018
Available online 15 November 2018
0038-092X/

upturn but not linear-like upward bend of the illuminated *I–V* characteristics in the first quadrant. Subsequently, to seek further generalization, De Castro et al. (2016) and Roland et al. (2016) published the corresponding modifications of the previous model (García-Sánchez et al., 2013) to gain insight into the modelling and parametrization of OSC current-voltage curves. In general, it is not mathematically possible to obtain an analytical solution to the above two models (De Castro et al., 2016; Roland et al., 2016). Therefore, numerical iteration or approximate methods are commonly used to solve the above two models, where numerical iteration solutions consume much computation time and approximate method solutions easily reduce computation accuracy. Finally, Xu et al. (2018) and Huang et al. (2018) improved B. Mazhari's model to simulate the linear-like S-shaped kink probably existing in the third quadrant.

The fundamental novelty of this paper is proposing an improved three-diode lumped-parameter equivalent circuit model of OSCs. Such a model can visualize the overall shape of the S-shaped *I-V* characteristics, thus facilitating us to give further researches on underlying physical phenomena of OSCs. The immediate contribution of this paper is deriving the explicit solution of the proposed model to avoid the need for numerical iteration or approximate method solutions to express the OSCs' electrostatic performance. The explicit solutions to our model help to easily extract the fitting parameters, significantly speed up the process of simulating OSCs' *I-V* characteristics, and promptly analyze the effects from the model parameters. Finally, the method of least squares, Newton-Raphson root-finding scheme, and the measured *I-V* data of OSCs validate the explicit solution to our proposed model. Good verification results illustrate that our proposed model can accurately reproduce the S-shaped *I-V* plots of OSCs and the derived explicit solution can implement compactly our model into simulations of OSCs' applications.

2. Proposed lumped-parameter model of organic solar cells

The previous lumped-parameter equivalent circuit model proposed by Mazhari (2006) includes only six parameters resulting from three diodes, as shown in Fig. 1. Compared with inorganic solar cells, excitons instead of free carriers are created in organic solar cells (OSCs). These excitons subsequently diffuse to the interface between donor and acceptor films and dissociate to form polaron-pairs. After the generation of polaron-pairs, they either recombine to form recombination current I_R or be extracted by electrodes to form extraction current I_E. In addition, I_D is the dark current of the device in the absence of light. For a given light intensity, I_{ph} is the current representing the polaron-pair generation rate. I and V are the terminal current and voltage of the OSCs, respectively. In fact, the terminal current depends on competition between polaron recombination and its collection by the electrodes. Because the free charge collection or extraction efficiency depends on internal electric field, it is expected that current would, in general, depend on voltage across the device.

In Mazhari's model, as shown in Fig. 1, current source I_{ph} demonstrates the net polaron generation rate, which is a constant in the case of a fixed light intensity. The diodes, D_R, D_E, and D_D model the loss of

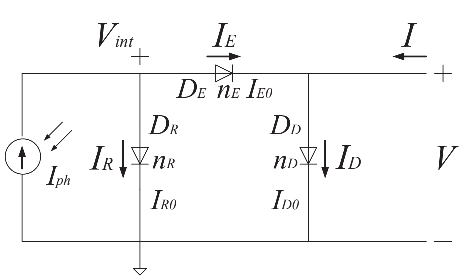

Fig. 1. The organic solar cells' lumped-parameter equivalent circuit model (Mazhari, 2006) proposed by B. Mazhari.

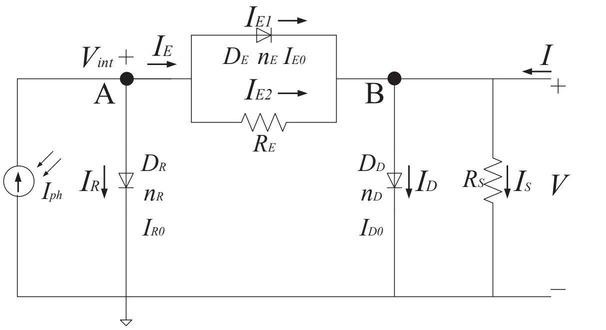

Fig. 2. The improved lumped-parameter equivalent circuit model of organic solar cells.

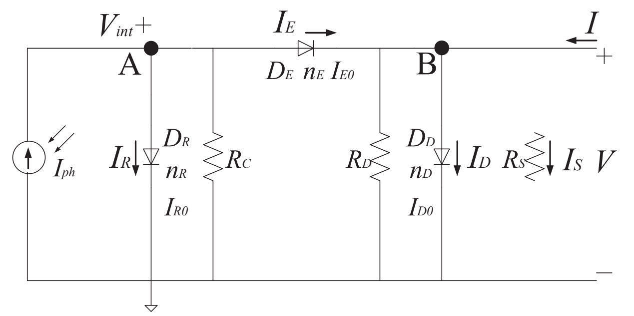

Fig. 3. The equivalent lumped-parameter circuit with Fig. 2 according to Miller theorem.

polarons due to recombination, the extraction due to internal electric field, and the *I-V* characteristics of the OSCs in the absence of light, respectively. Mazhari's model can both qualitatively and quantificationally analyze the electrical properties of OSCs, especially for the S-shaped *I-V* characteristics. It is noted that there are not any series or shunt resistances in Mazhari's model. As a result, the simulations of Mazhari's model for OSCs are not enough accurate in the first and third quadrants (Xu et al., 2018; Huang et al., 2018).

In this paper, we improve Mazhari's model by adding two shunt resistances R_E and R_s as shown in Fig. 2. From mathematical aspects, the shunt resistances R_E and R_s are used to improve the accuracy of the simulations for OSCs' S-shaped *I-V* characteristics. From physical aspects, both D_E and R_E instead of only D_E model the extraction current I_E of free carriers following the dissociation of polarons. In addition, R_S is used to describe the parasitic resistance in OSCs.

From circuit aspects, according to Miller theorem, the lumped-parameter circuit in Fig. 2 can be transformed into the following circuit as shown in Fig. 3. However, two more shunt resistances $R_C = \frac{V_{int} \cdot R_E}{V_{int} - V}$ and $R_D = -\frac{V \cdot R_E}{V_{int} - V}$ are added into Mazhari's model. Obviously, the lumped-parameter equivalent circuit model of OSCs including only two shunt resistances in Fig. 2 is simpler than that in Fig. 3. Simultaneously, the circuit in Fig. 2 also assures the accuracy of simulations for OSCs' S-shaped characteristics.

3. Model's equation explicit solution

Our improved lumped-parameter equivalent circuit by adding R_E is to predict accurately the S-shaped *I-V* characteristics of OSCs, as shown in Fig. 2. At points A and B, applying Kirchhoff's current law to the circuit of Fig. 2, we can obtain

$$I_{ph} = I_R + I_E, \tag{1}$$

$$I = I_D + I_S - I_E. \tag{2}$$

Subsequently, we substitute the standard diode equation (Shockley, 1949) into (1) and (2), yielding

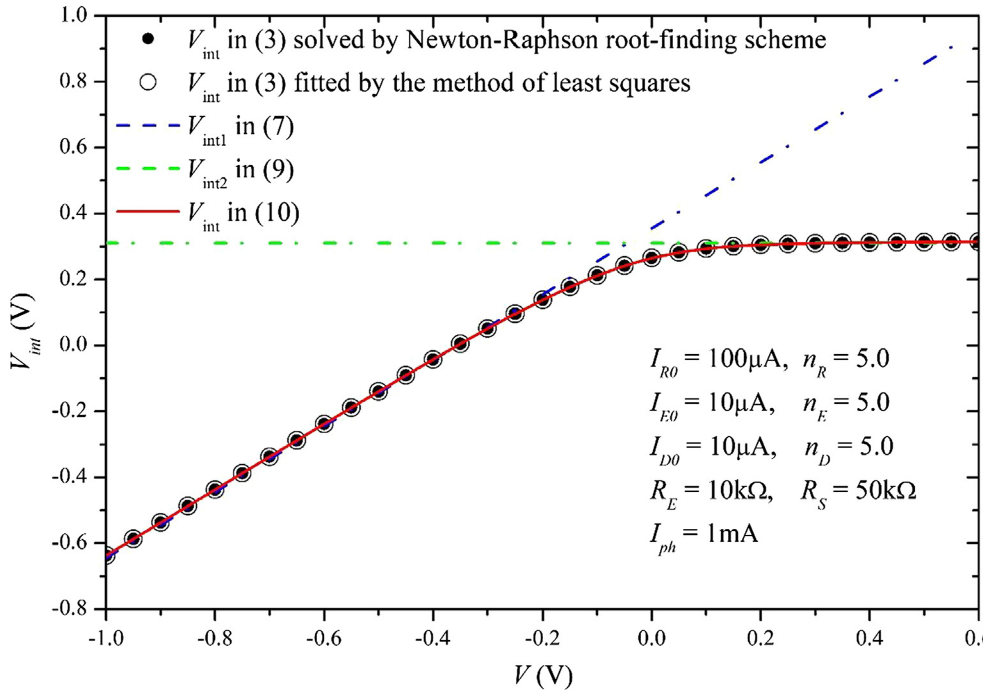

Fig. 4. V_{int} *vs.* V in our equivalent lumped-parameter circuit of Fig. 2.

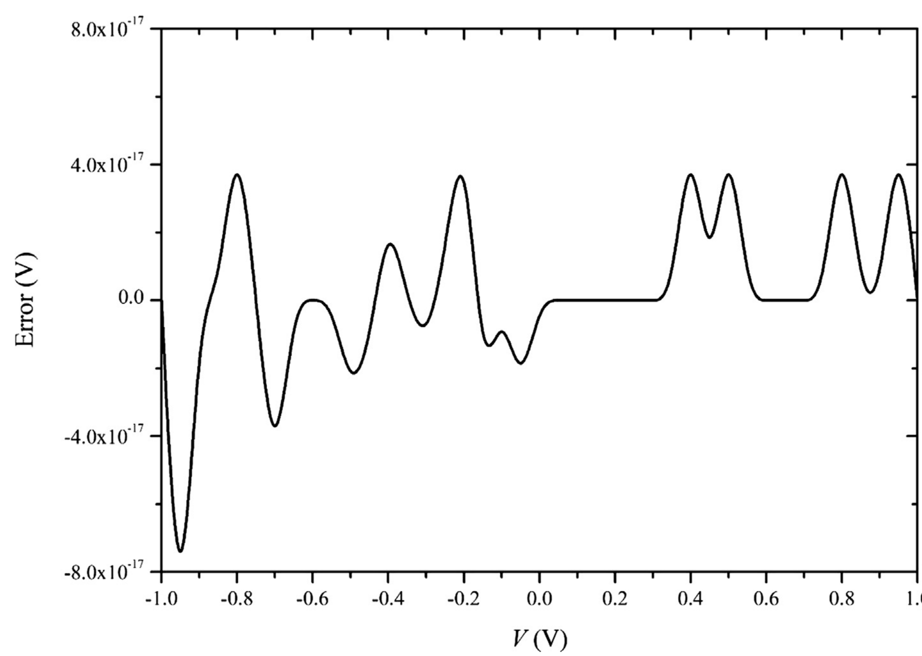

Fig. 5. Errors between V_{int} calculated in (10) and V_{int} in (3) fitted in the method of least squares.

$$I_{ph} = I_{R0}\left(e^{\frac{V_{\text{int}}}{n_R V_t}} - 1\right) + \left[I_{E0}\left(e^{\frac{V_{\text{int}}-V}{n_E V_t}} - 1\right) + \frac{V_{\text{int}} - V}{R_E}\right], \tag{3}$$

$$I = I_{D0}\left(e^{\frac{V_{\text{int}}}{n_D V_t}} - 1\right) + \frac{V}{R_S} - \left[I_{E0}\left(e^{\frac{V_{\text{int}}-V}{n_E V_t}} - 1\right) + \frac{V_{\text{int}} - V}{R_E}\right]. \tag{4}$$

If we look forward to solving the *I-V* characteristics of OSCs, combining (3) and (4) to eliminate V_{int} is necessary for deriving the relationship between I and V, which is also the transcendental function (Romero et al., 2017). This process is too complicated to solve analytically the expression I as a function of V. Of course, in our previous works (Xu et al., 2018; Huang et al., 2018), we avoid to directly solve the expression of I from the transcendental function. On the contrary, we firstly derive V_{int} from (3) through the Newton-Raphson root-finding method, and then we secondly substitute the results of V_{int} into (4) to obtain the *I-V* characteristics of OSCs. After all, the Newton-Raphson root-finding method is a kind of numerical iteration method, which consumes amount of computational time, leading to the poor computational efficiency. In this paper, in order to improve the computational efficiency, we analytically derive the expression of V_{int} from (3) through the regional approach, which is to be shown as follows.

In the case of backward terminal voltage V, the internal electric field existing in OSCs collects and extracts the free charges resulting from polaron-pairs. From the view of physical significance, in Fig. 2, the extraction current I_E is much larger than the recombination current I_R. From the view of mathematical computation, in (3),

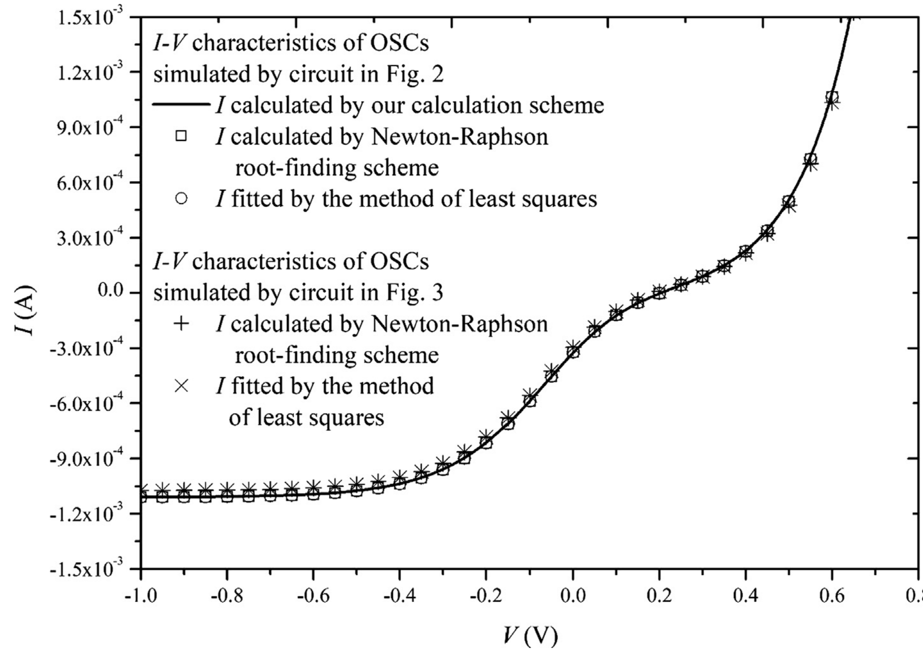

Fig. 6. I *vs.* V simulated by lumped-parameter circuits in Figs. 2 and 3.

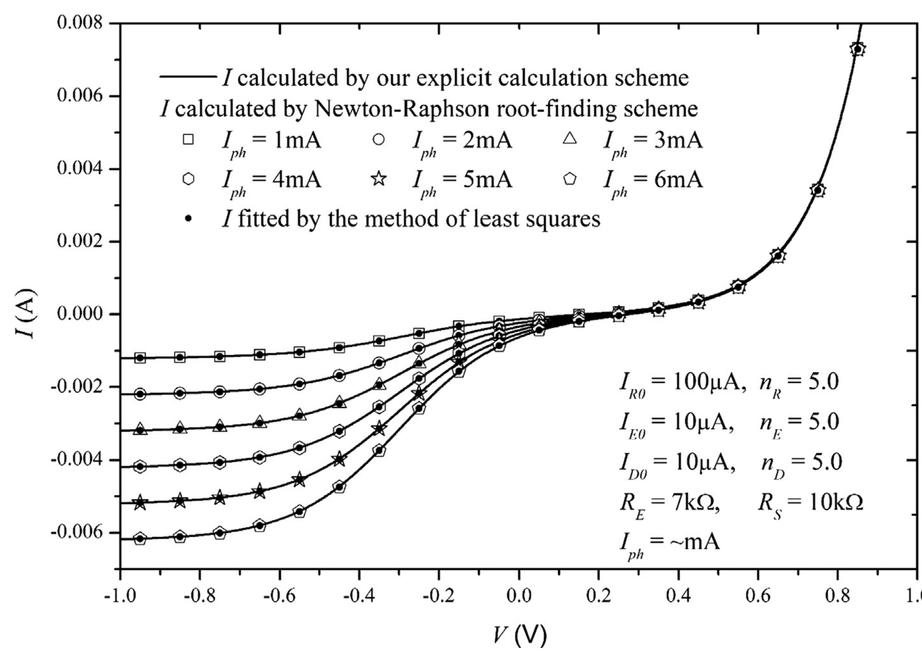

Fig. 7. Effects from I_{ph} on I-V characteristics of OSCs simulated by our lumped-parameter circuits.

$\left[I_{E0}\left(e^{\frac{V_{int}-V}{n_E V_t}}-1\right)+\frac{V_{int}-V}{R_E}\right]$ representing I_E is the dominant item in the right hand side (RHS) of (3). Considering the condition that $\left[I_{E0}\left(e^{\frac{V_{int}-V}{n_E V_t}}-1\right)+\frac{V_{int}-V}{R_E}\right] \gg I_{R0}\left(e^{\frac{V_{int}}{n_R V_t}}-1\right)$, we can simplify (3) as

$$I_{ph}=I_{E0}\left(e^{\frac{V_{int1}-V}{n_E V_t}}-1\right)+\frac{V_{int1}-V}{R_E}. \qquad (5)$$

Here, V_{int1} is the asymptotic solution of V_{int} in (3). It is noted that (5) is only valid for the case of large backward terminal voltage V, because we neglect the item $I_{R0}\left(e^{\frac{V_{int}}{n_R V_t}}-1\right)$ in (3). Now, only one exponent item is included in (5). Therefore, we can reformulate (5) as the typical mathematical formula of the lambert W function (Corless et al., 1996), i.e.,

$$\left[\frac{R_E(I_{ph}+I_{E0})}{n_E V_t}-\frac{V_{int1}-V}{n_E V}\right]\cdot\exp\left[\frac{R_E(I_{ph}+I_{E0})}{n_E V_t}-\frac{V_{int1}-V}{n_E V_t}\right] = \frac{R_E I_{E0}}{n_E V_t}\cdot\exp\left[\frac{R_E(I_{ph}+I_{E0})}{n_E V_t}\right]. \qquad (6)$$

Furthermore, we can derive the expression of V_{int1} from (6) as

$$V_{int1}=V+R_E(I_{ph}+I_{E0})-n_E V_t\cdot W_0\left[\frac{R_E I_{E0}}{n_E V_t}\cdot\exp\left(\frac{R_E I_{ph}+R_E I_{E0}}{n_E V_t}\right)\right]. \qquad (7)$$

Here, W_0 is the Lambert W function's principal branch (Corless et al., 1996), as a typical solution to equation $W_0(x)e^{W_0(x)}=x$.

In the case of forward terminal voltage V, the internal electric field existing in OSCs is not enough strong to collect polaron-pairs by two electrodes, i.e., anode and cathode. From the view of physical

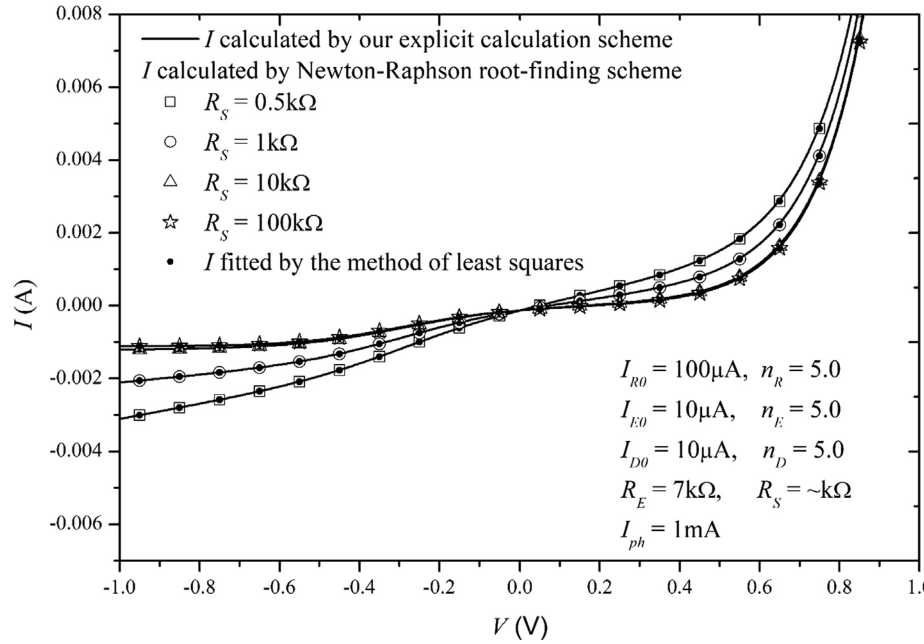

Fig. 8. Effects from R_S on *I-V* characteristics of OSCs simulated by our lumped-parameter circuits.

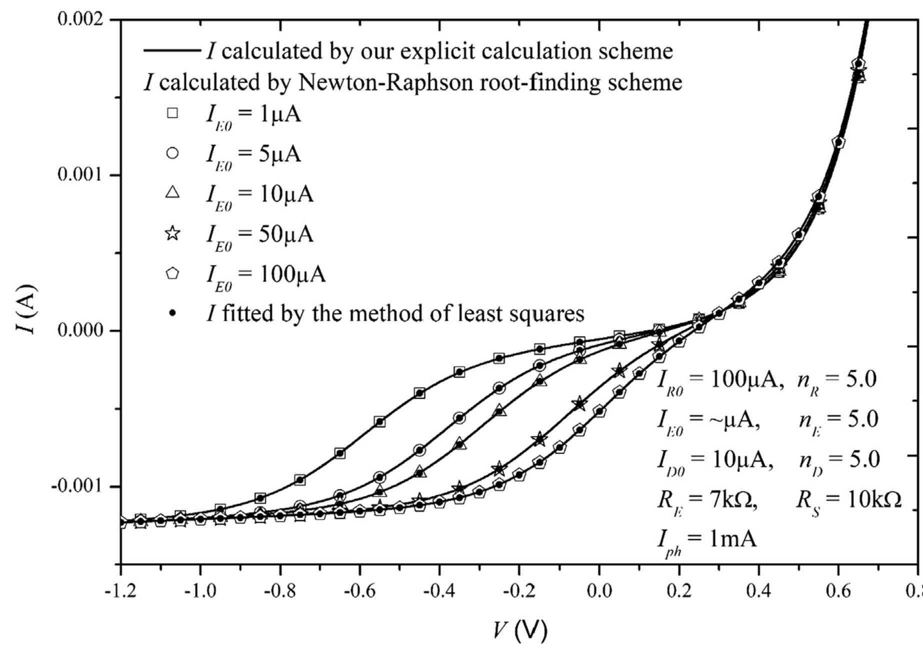

Fig. 9. Effects from I_{E0} on *I-V* characteristics of OSCs simulated by our lumped-parameter circuits.

significance, in Fig. 2, I_R is much larger than I_E. From the view of mathematical computation, $I_{R0}\left(e^{\frac{V_{int}}{n_R V_t}}-1\right)$ is the dominant item in the RHS of (3). Considering the condition that $I_{R0}\left(e^{\frac{V_{int}}{n_R V_t}}-1\right) \gg \left[I_{E0}\left(e^{\frac{V_{int}-V}{n_E V_t}}-1\right)+\frac{V_{int}-V}{R_E}\right]$, we can simplify (3) as

$$I_{ph} = I_{R0}\left(e^{\frac{V_{\text{int}2}}{n_R V_t}}-1\right). \tag{8}$$

Here, $V_{\text{int}2}$ is the asymptotic solution of V_{int} in (3). It is noted that (8) is only valid for the case of forward terminal voltage V, because we neglect the item $\left[I_{E0}\left(e^{\frac{V_{int}-V}{n_E V_t}}-1\right)+\frac{V_{int}-V}{R_E}\right]$ in (3). We can derive the expression of $V_{\text{int}2}$ from (8) as

$$V_{\text{int}2} = n_R V_t \cdot \ln\left(\frac{I_{ph}}{I_{R0}}+1\right). \tag{9}$$

In order to obtain the results of V_{int} valid for the whole operational region of OSCs (i.e., including both backward and forward terminal voltage V), we use the smoothing function to connect the expressions $V_{\text{int}1}$ and $V_{\text{int}2}$ and Schroder series to improve the accuracy of V_{int}, yielding

$$V_{\text{int}} = \frac{1}{10}\cdot\ln\left[\frac{1}{1/\exp(10\cdot V_{\text{int}1})+1/\exp(10\cdot V_{\text{int}2})}\right]+\omega. \tag{10}$$

Here, we modify the starting function V_{int} in (10) by adding the correction of Schroder series ω (Deng et al., 2014; Yu et al., 2016), which is symbolled as $\omega = (y/y')/(1-0.5yy''/y'/y')$, where

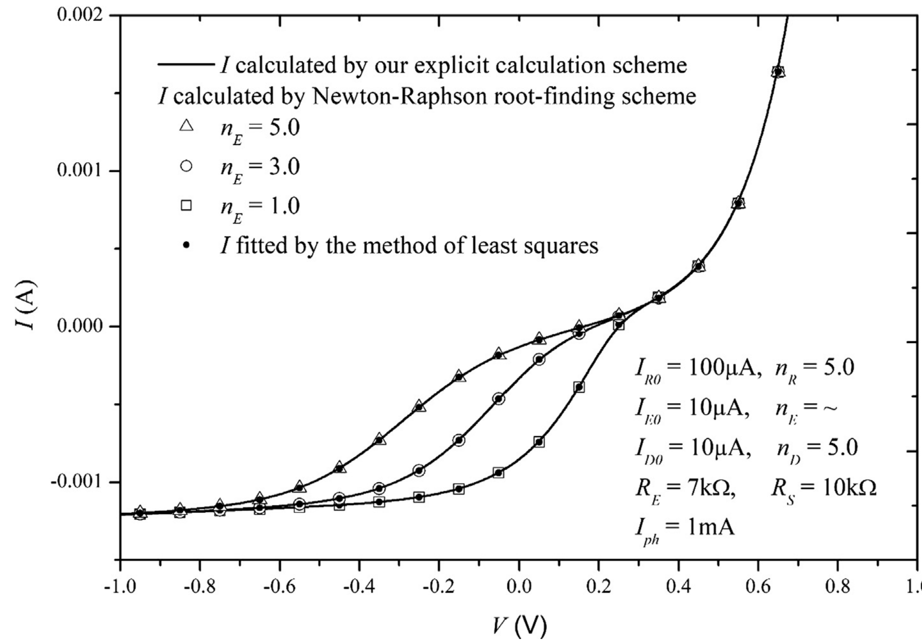

Fig. 10. Effects from n_E on *I-V* characteristics of OSCs simulated by our lumped-parameter circuits.

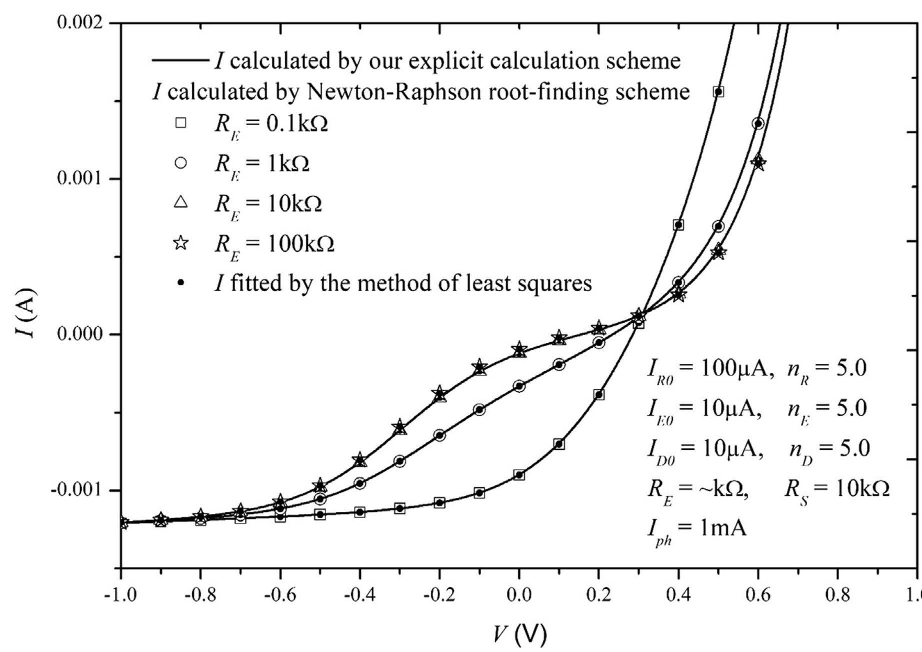

Fig. 11. Effects from R_E on *I-V* characteristics of OSCs simulated by our lumped-parameter circuits.

$y = I_{R0}\left(e^{\frac{V_{int}}{n_R V_t}} - 1\right) + \left[I_{E0}\left(e^{\frac{V_{int}-V}{n_E V_t}} - 1\right) + \frac{V_{int}-V}{R_E}\right] - I_{ph}$, y′ is the first derivative of y versus V_{int} with $y' = \frac{I_{R0}}{n_R V_t} \bullet e^{\frac{V_{int}}{n_R V_t}} + \frac{I_{E0}}{n_E V_t} \bullet e^{\frac{V_{int}-V}{n_E V_t}} + \frac{1}{R_E}$, and y″ are the second derivative of y versus V_{int} with $y'' = \frac{I_{R0}}{(n_R V_t)^2} \bullet e^{\frac{V_{int}}{n_R V_t}} + \frac{I_{E0}}{(n_E V_t)^2} \bullet e^{\frac{V_{int}-V}{n_E V_t}}$. In fact, the method that deriving the starting function and then modifying it with Schroder series has been regarded as a universal fashion (Deng et al., 2014; Yu et al., 2016).

In Fig. 4, we show V_{int1}-V, V_{int2}-V, and V_{int}-V characteristics. According to analysis of (7), V_{int1} is only suitable for the case of backward terminal voltage V. That is consistent with the results of V_{int} on the condition that $V < 0$ V, as shown in Fig. 4. According to analysis of (9), V_{int2} is only suitable for the case of forward terminal voltage V. That is also identical to the results of V_{int} on the condition that $V > 0$ V, as shown in Fig. 4. Of course, there is a transition region, where both I_R and I_E are not the dominant item in RHS of (3). Therefore, in this transition region, neither V_{int1} nor V_{int2} agree with V_{int} calculated through the Newton-Raphson root-finding scheme and the method of least squares from (3). However, by using smoothing function to choose the smaller value between V_{int1} and V_{int2}, and then, using Schroder series to improve the accuracy of computation results, we derive the explicit expression of V_{int} from (3) in this paper. It is noted that V_{int} calculated in (10) has a good match with the numerical iteration results of V_{int} in Fig. 4, especially for the transition region. In addition, Fig. 5 shows that the errors come into the scale of 10^{-16} V.

Substituting (10) into (4), we can obtain the explicit calculation scheme of OSCs' *I-V* characteristics. Furthermore, we show and compare the *I-V* characteristics of OSCs simulated by equivalent circuits in Figs. 2 and 3. We can observe from Fig. 6 that the simulation results of

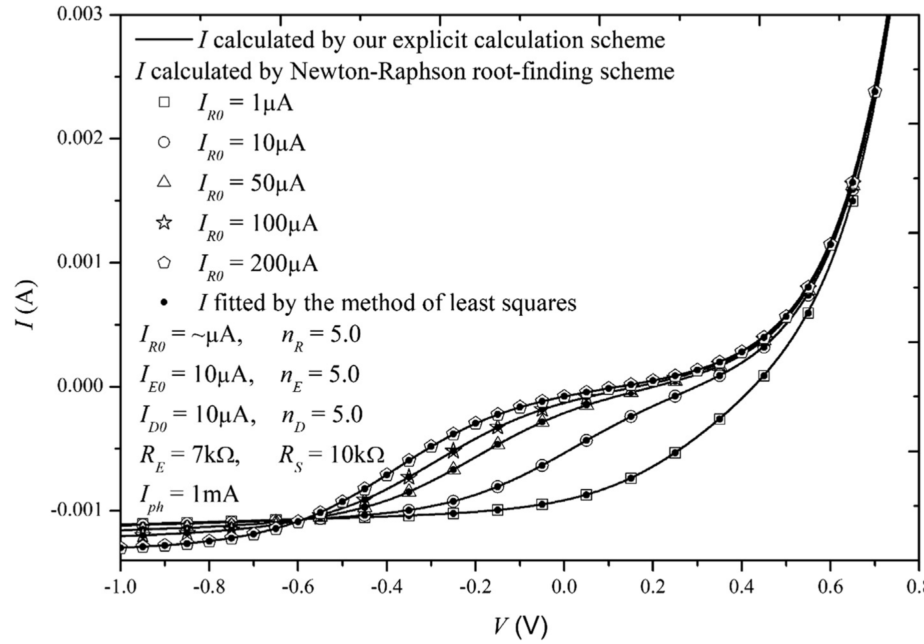

Fig. 12. Effects from I_{R0} on *I-V* characteristics of OSCs simulated by our lumped-parameter circuits.

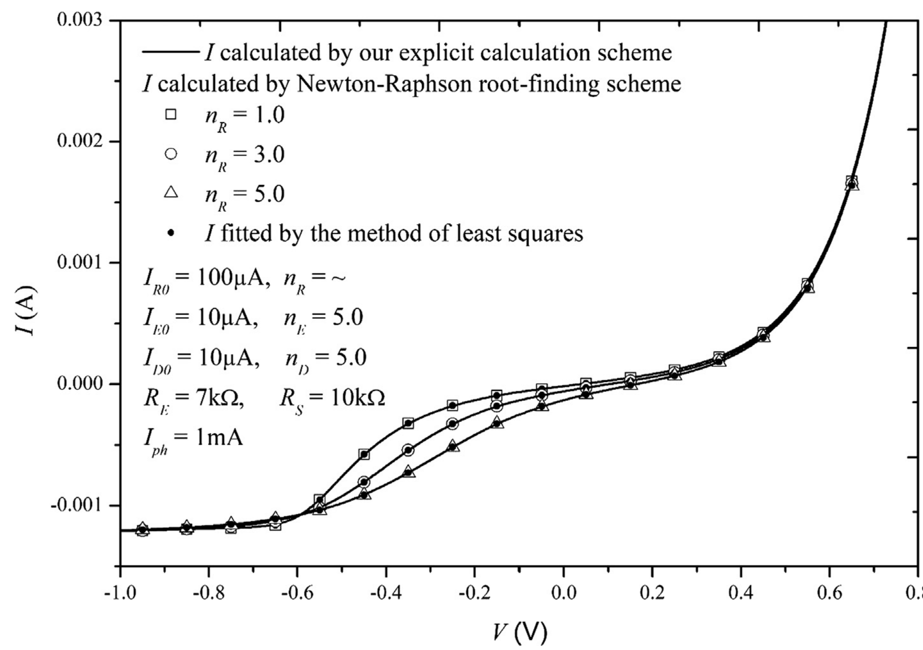

Fig. 13. Effects from n_R on *I-V* characteristics of OSCs simulated by our lumped-parameter circuits.

OSCs' *I-V* characteristics obtained from the lumped-parameter circuits in Figs. 2 and 3 are nearly consistent with each other. In other words, the circuits in Figs. 2 and 3 are equivalent. Of course, we also choose the simpler circuit in Fig. 2 instead of that in Fig. 3 to complete the simulations for the S-shaped *I-V* characteristics of OSCs.

4. Verification and discussion

A. Numerical iteration verification and discussion about fitting parameter effects

In this section, we use the method of least squares and Newton-Raphson root-finding scheme to fit and calculate the terminal current–voltage characteristics in Fig. 2, i.e., equation set of (3) and (4). And then, we use our explicit calculation scheme presented in Part 3 to solve V_{int} from (3) and substitute V_{int} into (4) to obtain *I-V* characteristics. Furthermore, we compare our results with numerical iteration results and discuss about the effects of the fitting parameters in Fig. 2 on the S-shaped *I-V* characteristics of OSCs.

The current source I_{ph} in Fig. 2 describes the net polaron generation rate of OSCs under illumination. In the cases of the different illumination intensities, I_{ph} proportional to illumination intensity influent directly the *I-V* characteristics in the third quadrant, as shown in Fig. 7. Obviously, the *I-V* curves shift downward as illumination intensity increases. It is noted that the offsets of the *I-V* curves in the third quadrant for I_{ph} result from the shunt resistance R_S. In Fig. 8, R_S determines the slope of the *I-V* curve in the third quadrant and the terminal current magnitude of the *I-V* curve in the first quadrant. On the one hand, the

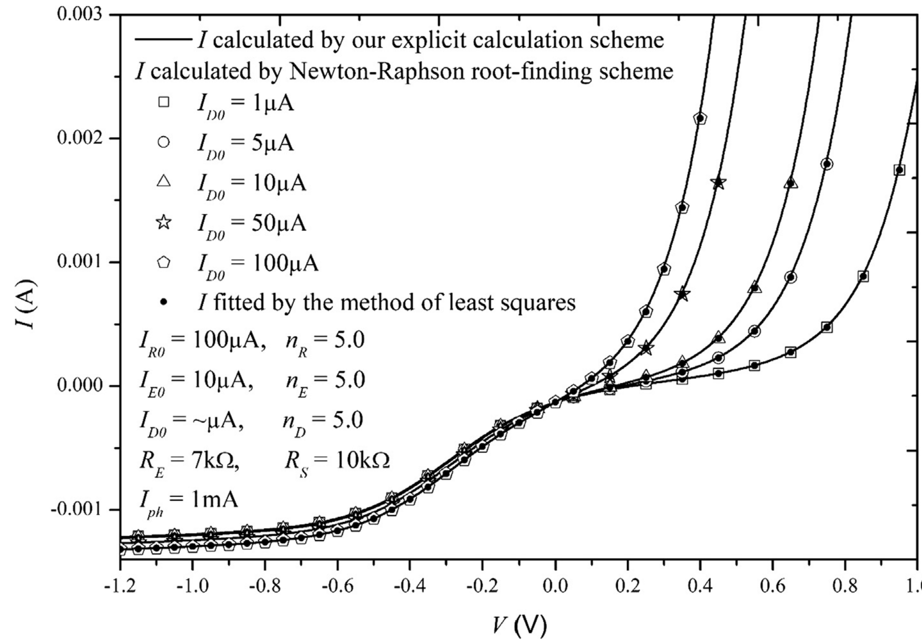

Fig. 14. Effects from I_{D0} on *I-V* characteristics of OSCs simulated by our lumped-parameter circuits.

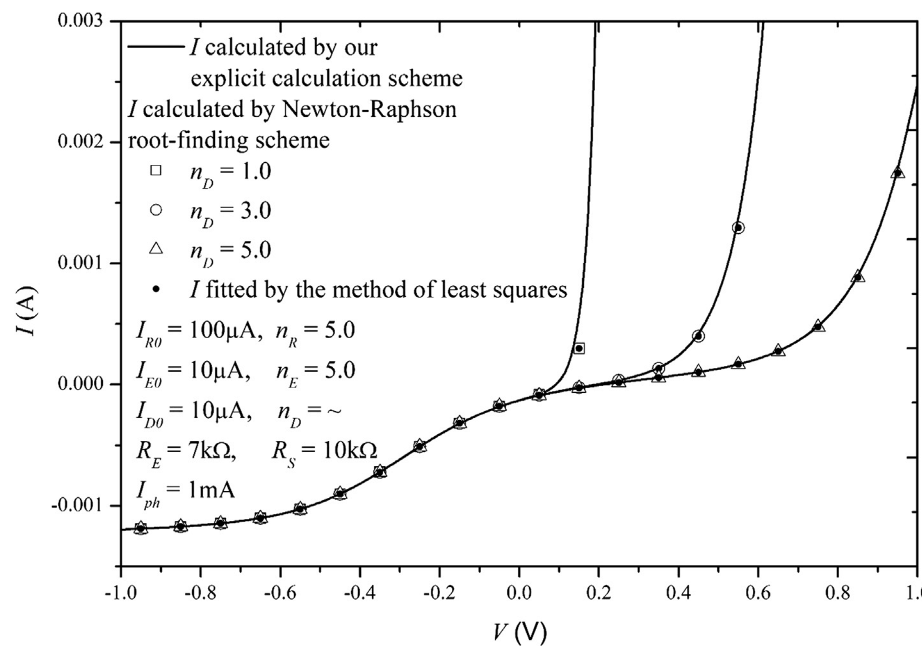

Fig. 15. Effects from n_D on *I-V* characteristics of OSCs simulated by our lumped-parameter circuits.

slope of the *I-V* curve decreases with the increment of R_S in the third quadrant. On the other hand, the terminal current magnitude of the *I-V* curve also decreases with the increment of R_S in the third quadrant. In a word, we can observe from Fig. 8 that there is a negative correlation between the shunt resistance R_S and power-conversion efficiency (PCE). In fact, R_S represents contract resistance of OSCs resulting from the interfaces between electrode and acceptor, between acceptor and donor, and between donor and electrode.

Compared with Mazhari's model (Mazhari, 2006) and our previous work (Xu et al., 2018), the main difference of our lumped-parameter equivalent circuit model is that the diode D_E in connection with the parallel resistance R_E represents the extraction current I_E, i.e., the sum of I_{E1} and I_{E2} in Fig. 2. In Figs. 9–11, we show that the parameters I_{E0}, n_E, and R_E have influences on the S-shaped *I-V* characteristics of OSCs. According to Figs. 9 and 10, both I_{E0} and n_E affect the *I-V* characteristics in the third quadrant. Obviously, large I_{E0} and small n_E can make the S-shaped *I-V* characteristics of OSCs approach into the J-shape, which would lead to higher PCE. Of course, that is consistent with the device physics. Both large I_{E0} and small n_E result in large extraction current, corresponding to large PCE. Compared with functions of I_{E0} and n_E, R_E also play an important role in increasing the extraction current of OSCs with the decrease of R_E. As shown in Fig. 11, in the case of small R_E, the *I-V* curve is J-shape leading to relative large PCE of OSCs. However, as R_E increases, the extraction current decreases. That would reduce the PCE of OSCs. As a result, the *I-V* curve would deviate J-shape and transfer into S-shape, as shown in Fig. 11. It is noted that D_E only influent those in the third quadrant, and R_E can affect the *I-V* curves in the first and third quadrants. In actual OSCs, *I-V* characteristics in the first

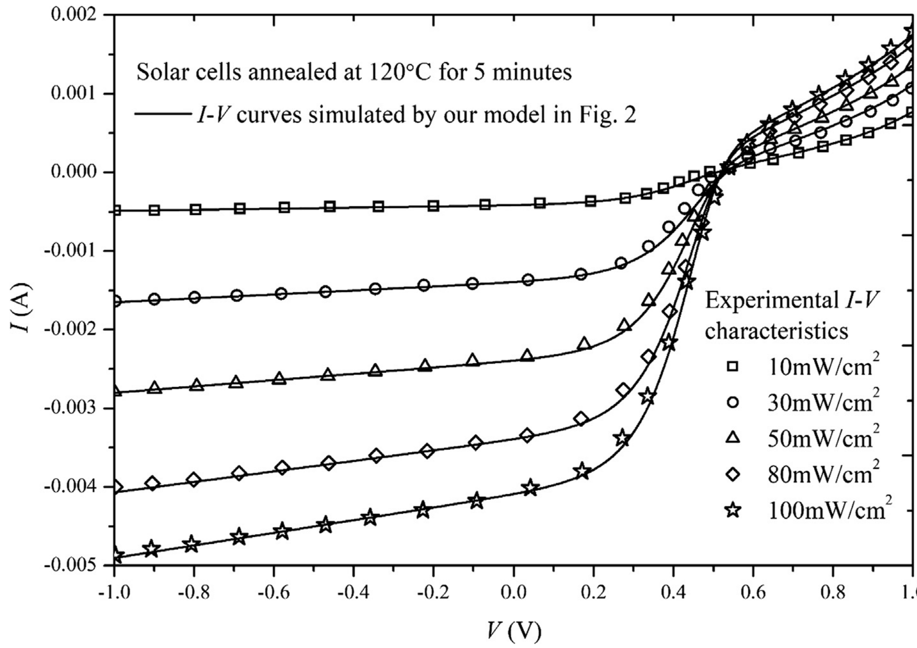

Fig. 16. *I-V* characteristics of OSCs annealed at 120 °C for 5 min, simulated by our model and measured in (Laudani et al., 2018).

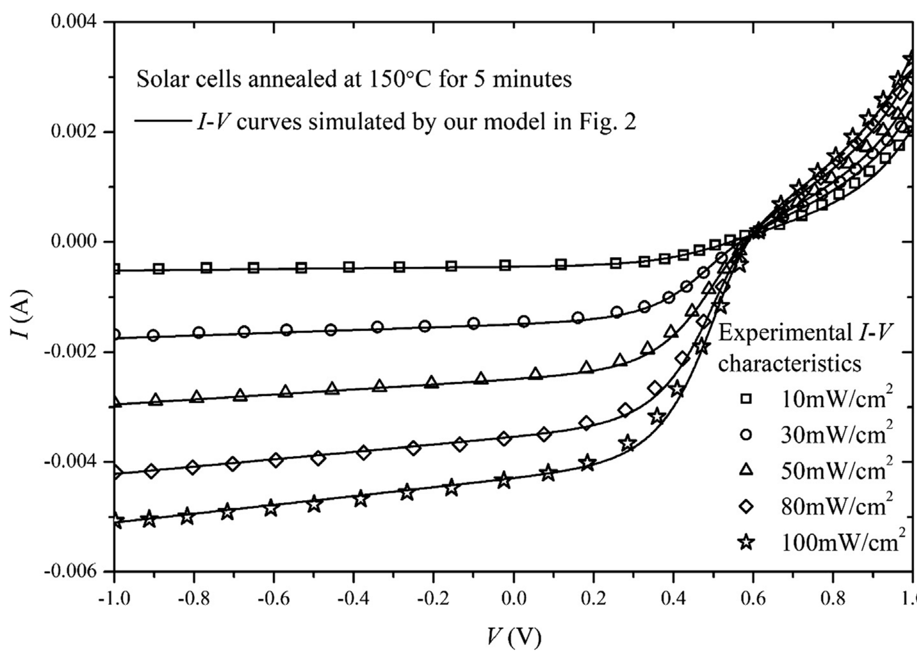

Fig. 17. *I-V* characteristics of OSCs annealed at 150 °C for 5 min, simulated by our model and measured in (Laudani et al., 2018).

quadrant is exponent-like rise instead of exponent rise described by only one diode D_E Mazhari's model (Mazhari, 2006) and our previous model (Xu et al., 2018). In this paper, we use both the diode D_E and the shunt resistance R_E to demonstrate the extraction current. If R_E tends towards infinity, the lumped-parameter circuit degrades into Mazhari's model (Mazhari, 2006) and our previous model (Xu et al., 2018) so that the *I-V* curves in the first quadrant approach to exponent rise. If R_E tends towards zero, I_{E2} would be much larger than I_{E1} in Fig. 2 so that the *I-V* curves in the first quadrant approach to line rise.

The Diode D_R simulates the recombination current of OSCs and Figs. 12 and 13 show that the effects of I_{R0} and n_R on the *I-V* characteristics. In contrast to the effects of D_E, the larger recombination current through D_R leads to low PCE of OSCs. In Figs. 12 and 13, for smaller I_{R0} and larger n_R, PCE is larger. The Diode D_D simulates the dark current of OSCs and Figs. 14 and 15 show that the effects of I_{D0} and n_D on the *I-V* characteristics. According to Figs. 14 and 15, large I_{D0} and small n_D can lead to large I_D corresponding with large PCE.

B. Experiment verification

In Figs. 16–20, we compare the *I-V* characteristics simulated by our proposed lumped-parameter circuit in Fig. 2 with the reconstructed experimental data (Laudani et al., 2018) of OSCs and obtain the good agreements on the different conditions of annealing temperature and illumination intensity. The fitting parameters used in simulations are listed in Table 1., that can be extracted through the common routine of the parameter acquisition (Mazhari, 2006). We make use of organic solar cells (Laudani et al., 2018), consisting of an enhanced bi-layer of

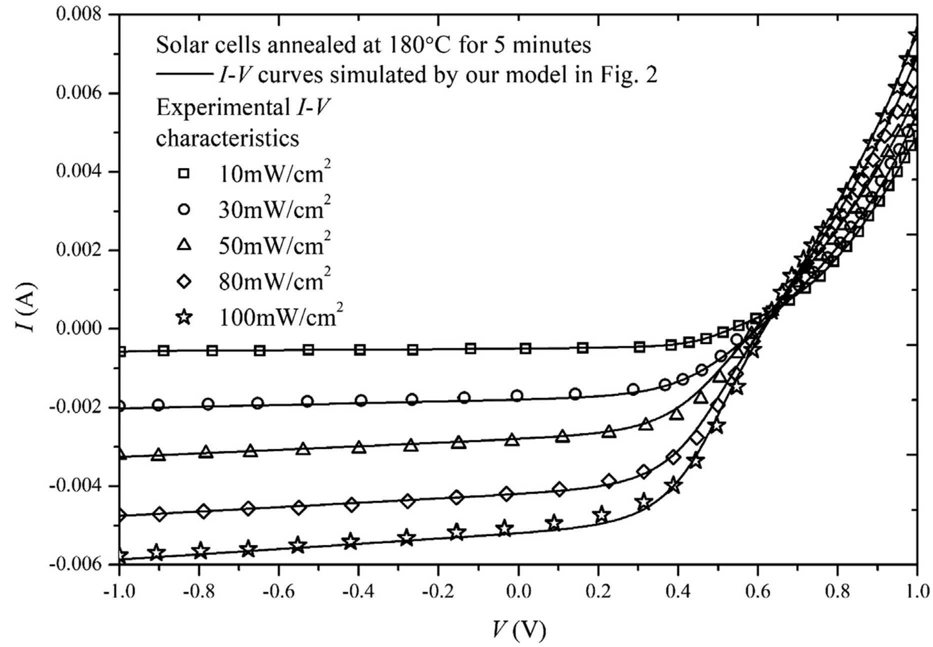

Fig. 18. *I-V* characteristics of OSCs annealed at 180 °C for 5 min, simulated by our model and measured in (Laudani et al., 2018).

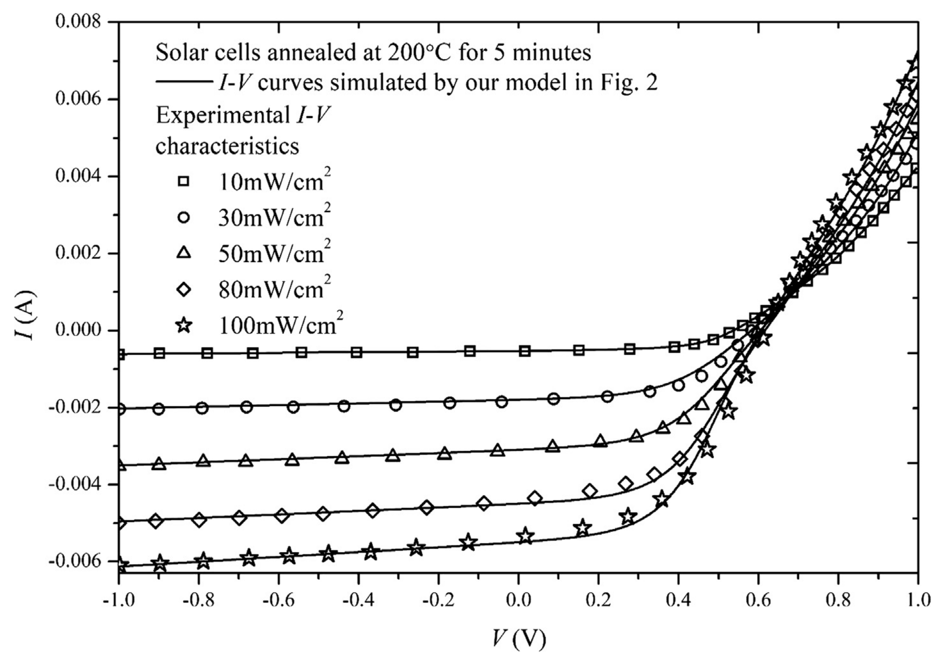

Fig. 19. *I-V* characteristics of OSCs annealed at 200 °C for 5 min, simulated by our model and measured in (Laudani et al., 2018).

purified Poly[2-methoxy-5-(2-ethylhexyloxy)-1,4-phenylene-vinylene] (MEH-PPV, M_n = 40,000–70,000, Aldrich) acting as electron donor and fullerene C60 (> 99.95%, SES Research) acting as electron acceptor. Films were fabricated on cleaned ITO-coated glass coated with 50 nm of PEDOT:PSS (Aldrich, conductivity 1 S cm^{-1}) and subsequently coated with 50 nm of Al to serve as the cathode.

Under the N_2 atmosphere, the OSCs were exposed to the different illumination intensities (i.e., 10 mW/cm^2, 30 mW/cm^2, 50 mW/cm^2, 80 mW/cm^2, 100 mW/cm^2) simulated AM1.5G sunlight, and the *I–V* characteristics were measured and shown as symbols in Figs. 16–19. It is noted that larger illumination intensity in measurement needs larger I_{ph} in our model to complete simulating the *I-V* characteristics of OSCs. In addition, we can observe from Fig. 20 that higher thermal annealing temperature can be used to reduce the S-shape, leading to higher PCE of OSCs.

5. Conclusions

In this paper, we proposed an improved lumped-parameter equivalent circuit model of organic solar cells to give the accurate descriptions about the S-shaped *I-V* characteristics. Firstly, we present the circuit structure of the lumped-parameter model and its equivalent circuit following Miller theorem. Secondly, we derive the explicit expression of the *I-V* characteristics based on the regional approach. Thirdly, we verify the simulation results of our model by using Newton-Raphson root-finding scheme and the method of least squares and discuss about effects from fitting parameters on the *I-V* curves of OSCs. Finally, we compare simulation results with reconstructed experimental

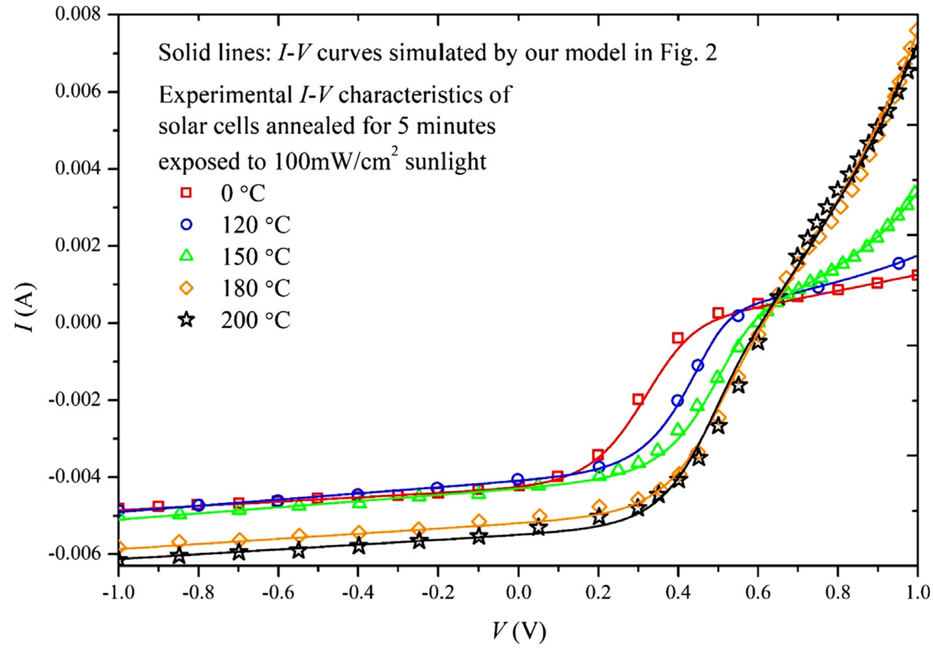

Fig. 20. *I-V* characteristics of OSCs annealed different temperatures, simulated by our model and measured in (Laudani et al., 2018).

Table 1
Parameters for simulations of our model.

Symbol (units)	No annealing	Annealing at 120 °C	Annealing at 150 °C	Annealing at 180 °C	Annealing at 200 °C
Illumination (mW/cm^2)	–	10,30,50,80,100	10,30,50,80,100	10,30,50,80,100	10,30,50,80,100
I_{R0} (μA)	2.5	2.5	2.0	2.0	2.0
I_{E0} (μA)	30	30	30	30	30
I_{D0} (nA)	0.012	12	15	15	15
n_R	2.9	4, 3.5, 3.2, 3.1, 3.0	4, 3.5, 3.4, 3.3, 3.2	4, 3.5, 3.3, 3.2, 3.1	4, 3.4, 3.3, 3.1, 3.0
n_E	1.8	1.0	1.0	1.0	1.0
n_D	6.2	4.0	3.5	3.5	3.5
R_E (kΩ)	0.65	0.8,0.6,0.55,0.55,0.55	0.3,0.3,0.26,0.22,0.20	0.08,0.07,0.07,0.06,0.05	0.08,0.07,0.06,0.06,0.05
R_S (kΩ)	1.8	15, 4, 2.5, 1.5, 1.25	15, 4, 2.2, 1.5,1.25	10, 4.5, 2.2, 1.8, 1.5	10, 4.5, 2.5, 2.2, 1.6
I_{ph} (mA)	4.3	0.42, 1.4, 1.6, 3.4, 4.1	0.45, 1.5, 2.5, 3.5,4.3	0.5, 1.8, 2.8, 4.2, 5.2	0.5, 1.8, 3.5, 4.5, 5.5

data to valid our model. As a result, such a model can be adopted as the useful platform to electrically explain the S-shaped *I-V* characteristics of OSCs and complete computer-aided-design system of photovoltaic applications.

Acknowledgement

This work was funded partially by the Scientific Research Funds of Huaqiao University under grant 16BS706 and partially by the Scientific Research Funds for the Young Teachers of Fujian Province under grant JAT170034.

References

Chavali, R.V.K., Li, J.V., Battaglia, C., De Wolf, S., Gray, J.L., Alam, M.A., 2017. A generalized theory explains the anomalous suns-voc response of Si heterojunction solar cells. IEEE J. Photovolt. 7, 169–176.
Corless, R.M., Gonnet, G.H., Hare, D.E.G., Jeffrey, D.J., Knuth, D.E., 1996. On Lambert's W function. Adv. Comput. Math. 5, 329–359.
De Castro, F., Heier, J., Nüesch, F., Hany, R., 2010. Origin of the kink in current-density versus voltage curves and efficiency enhancement of polymer-c60 heterojunction solar cells. IEEE J. Sel. Top. Quant. Electron. 16, 1690–1699.
De Castro, F., Laudani, A., Riganti Fulginei, F., Salvini, A., 2016. An in-depth analysis of the modelling of organic solar cells using multiple-diode circuits. Sol. Energy 135, 590–597.
Deng, W., Huang, J., Ma, X., Ning, T., 2014. An explicit surface-potential-based model for amorphous IGZO thin-film transistors including both tail and deep states. IEEE Electron Dev. Lett. 35, 78–80.
Dominguez, I.F., Distler, A., Luer, L., 2017. Stability of organic solar cells: the influence of nanostructured carbon materials. Adv. Energy Mater. 7, 1601320.
García-Sánchez, F.J., Lugo-Muñoz, D., Muci, J., Ortiz-Conde, A., 2013. Lumped parameter modeling of organic solar cells' S-shaped I-V characteristics. IEEE J. Photovolt. 3, 330–335.
Gaur, A., Kumar, P., 2014. An improved circuit model for polymer solar cells. Prog. Photovolt: Res. Appl. 22, 937–948.
Huang, G., Yu, F., Xu, C., 2018. An analytical solution to lumped parameter equivalent circuit model of organic solar cells. Crystals 8, 224.
Kale, P.G., Solanki, C.S., 2015. Silicon quantum dot solar cell using top-down approach. International Nano Letters 5, 61–65.
Kumar, P., Gaur, A., 2013. Model for the J-V characteristics of degraded polymer solar cells. J. Appl. Phys. 113, 094505.
Laudani, A., Riganti Fulginei, F., De Castro, F., Salvini, A., 2018. Irradiance intensity dependence of the lumped parameters of the three diodes model for organic solar cells. Sol. Energy 163, 526–536.
Mazhari, B., 2006. An improved solar cell circuit model for organic solar cells. Sol. Energy Mater. Sol. Cells 90, 1021–1033.
Ortiz-Conde, A., García-Sánchez, F.J., Muci, J., Sucre-González, A., 2014. A review of diode and solar cell equivalent circuit model lumped parameter extraction. Facta Universitatis, Series: Electronics and Energetics 27, 57–102.
Roland, P.J., Bhandari, K.P., Ellingson, R.J., 2016. Electronic Circuit Model for Evaluating S-Kink. Distorted Current-Voltage Curves, *Proc. IEEE 43rd Photovoltaic Specialists Conf.* (PVSC).
Romero, B., del Pozo, G., Arredondo, B., Martín-Martín, D., Ruiz Gordoa, M.P., Pickering, A., Pérez-Rodríguez, A., Barrena, E., García-Sánchez, F.J., 2017. S-Shaped I-V characteristics of organic solar cells: solving Mazhari's lumped-parameter equivalent circuit model. IEEE Trans. Electron Dev. 64, 4622–4627.
Sanchez, J.G., Balderrama, V.S., Estrada, M., Osorio, E., Ferre-Borrull, J., Marsal, L.F., Pallares, J., 2017. Stability study of high efficiency polymer solar cells using TiOx as electron transport layer. Sol. Energy 150, 147–155.
Shockley, W., 1949. The theory of p-n junctions in semiconductors and p-n junction transistors. Bell Syst. Tech. J. 28, 435–489.
Tran, V.H., Ambade, R.B., Ambade, S.B., Lee, S.H., Lee, I.H., 2017. Low-temperature solution-processed SnO2 nanoparticles as cathode buffer layer for inverted organic

solar cells. ACS Appl. Mater. Interfaces 9, 1645–1653.

Wagenpfahl, A., Rauh, D., Binder, M., Deibel, C., Dyakonov, V., 2010. S-shaped current-voltage characteristics of organic solar devices. Phys. Rev. B 82, 115306.

Xu, C., Yu, F., Lin, W., Huang, G.Y., 2018. an improved organic solar cell lumped-parameter equivalent circuit model. Crystals 8, 277.

Yoshikawa, K., Kawasaki, H., Yoshida, W., Irie, T., Konishi, K., Nakano, K., Uto, T., Adachi, D., Kanematsu, M., Uzu, H., 2017. Silicon heterojunction solar cell with interdigitated back contacts for a photo conversion efficiency over 26%. Nat. Energy 2, 17032.

Yu, F., Deng, W., Huang, J., Ma, X., Chen, S., 2016. An explicit physics-based *I-V* model for surrounding-gate polysilicontransistors. IEEE Trans. Electron Devices 63, 1059–1065.

Zuo, L., Yao, J., Li, H., Chen, H., 2014. Assessing the origin of the S-shaped I-V curve in organic solar cells: an improved equivalent circuit model. Sol. Energy Mater. Sol. Cells 122, 88–93.